Evaluating Outer Tropical Cyclone Size in Reanalysis Datasets Using QuikSCAT Data

BENJAMIN A. SCHENKEL AND NING LIN

Department of Civil and Environmental Engineering, Princeton University, Princeton, New Jersey

DANIEL CHAVAS

Department of Earth, Atmospheric, and Planetary Sciences, Purdue University, West Lafayette, Indiana

MICHAEL OPPENHEIMER

Woodrow Wilson School of Public and International Affairs, and Department of Geosciences, Princeton University, Princeton, New Jersey

ALAN BRAMMER

Department of Atmospheric and Environmental Science, University at Albany, State University of New York, Albany, New York

(Manuscript received 24 February 2017, in final form 6 July 2017)

ABSTRACT

The present study examines the fidelity of outer tropical cyclone (TC) size and wind field structure in four atmospheric reanalysis datasets to evaluate whether reanalyses can be used to derive a long-term TC size dataset. Specifically, the precision and accuracy of reanalysis TC size for the North Atlantic (NA) and western North Pacific (WNP) basins are analyzed through comparison with a recently developed QuikSCAT TC size dataset (2000–09). Both outer TC size and structure in reanalyses closely match QuikSCAT data as revealed by strong correlations, similar standard deviations, and generally small biases. Of the TC size metrics examined, the radii of 6–8 m s^{-1} winds in the NA and radii of 6–10 m s^{-1} winds in the WNP are generally most comparable to QuikSCAT data. Compared to WNP TCs, NA TC size and structure are represented with greater fidelity. Among the four reanalyses examined, the National Centers for Environmental Prediction Climate Forecast System Reanalysis and the Japan Meteorological Agency Japanese 55-year Reanalysis represent TC size and structure with the greatest fidelity for both basins. Differences between reanalysis and QuikSCAT TC size increase with increasing QuikSCAT TC size in both basins and with decreasing TC latitude in the WNP. Finally, comparison of the distribution of reanalysis TC size during the satellite era with the distribution of QuikSCAT TC size suggests that reanalysis TC size is represented with reasonable fidelity throughout the satellite era and, thus, may be useful for constructing a multidecadal TC size dataset.

1. Introduction

Tropical cyclone (TC) size has been a topic of great interest given its association with TC intensity change (Carrasco et al. 2014), the physics and structure of the TC wind field (e.g., Chan and Chan 2013, 2014; Chavas and Emanuel 2014; Chavas et al. 2015; Chan and Chan 2015b; Chavas and Lin 2016), and TC wind and storm surge damage (e.g., Iman et al. 2005; Irish et al. 2008; Irish and Resio 2010; Lin et al. 2014; Zhai and Jiang 2014). Although prior studies have typically focused on the size of the inner TC circulation (i.e., radius of maximum winds), the outer TC circulation may be simpler to study given that it is more stable in time and it varies nearly independently from TC intensity (e.g., Merrill 1984; Chavas and Emanuel 2010; Lee et al. 2010; Chan and Chan 2012; Chavas et al. 2015; Chavas and Lin 2016). The outer region of the TC is defined as the broad circulation of the TC beyond the strongly convecting inner region that is nearly rain free and, thus, is approximately in radiative–subsidence balance (e.g., Emanuel 2004; Chavas et al. 2015).

Corresponding author: Benjamin A. Schenkel, benschenkel@gmail.com

DOI: 10.1175/JCLI-D-17-0122.1

© 2017 American Meteorological Society. For information regarding reuse of this content and general copyright information, consult the AMS Copyright Policy (www.ametsoc.org/PUBSReuseLicenses).

Unauthenticated | Downloaded 01/17/23 09:26 PM UTC

The size of the TC outer region has been typically defined using various radii of azimuthal-mean near-surface wind and pressure fields (e.g., Brand 1972; Merrill 1984; Liu and Chan 1999; Chavas and Emanuel 2010), with outer TC structure similarly represented using the radial structure of these azimuthal-mean fields (e.g., Emanuel 2004; Chavas and Emanuel 2014; Chavas et al. 2015; Chavas and Lin 2016). Specifically, the most commonly used outer TC size metrics include the radius of the outermost closed isobar (ROCI; e.g., Brand 1972; Merrill 1984; Kimball and Mulekar 2004) and the radius in which the azimuthal-mean lower-tropospheric azimuthal wind equals 5, 12, and 15 $m\,s^{-1}$ (e.g., Frank and Gray 1980; Chavas and Emanuel 2010; Knaff et al. 2014). Quantifying outer TC size may be particularly useful given that the structure and modes of variability of the complete azimuthal-mean near-surface TC wind field can be represented using a simple physical TC wind field model that only requires outer TC size and either TC intensity or the radius of maximum winds (Chavas et al. 2015; Chavas and Lin 2016). However, outer TC size has not been as extensively studied as TC intensity largely owing to 1) the absence of a long-term, objective, and observation-based outer TC size dataset until recently (e.g., Liu and Chan 1999; Chavas and Emanuel 2010; Knaff et al. 2014; Chan and Chan 2015a; Chavas et al. 2016) and 2) the difficulties in defining a physically meaningful outer TC size metric that can be uniformly derived across observational datasets (e.g., Brand 1972; Frank and Gray 1980; Liu and Chan 1999; Chavas and Emanuel 2010). With these facts in mind, the present study attempts to evaluate whether the current generation of atmospheric reanalysis datasets can provide a multidecadal, objective, and homogeneous outer TC size dataset derived from the outer TC wind field.

The earliest TC size studies utilized ROCI obtained from subjectively derived surface analyses (e.g., Brand 1972; Merrill 1984). However, the estimation of ROCI in these studies may have been negatively impacted by the sparsity of the input data in the surface analysis. Later work utilized either rawinsonde or in situ aircraft reconnaissance data to study the radius of 15 $m\,s^{-1}$ azimuthal-mean lower-tropospheric winds (e.g., Frank and Gray 1980; Weatherford and Gray 1988a,b), but these studies may have been adversely impacted by the heterogeneous sampling of TC winds in space and time. The introduction of scatterometer data allowed for subsequent research to examine various 10-m wind radii and vorticity thresholds as TC size metrics (e.g., Liu and Chan 1999; Chavas and Emanuel 2010; Chan and Chan 2015a; Chavas and Lin 2016). Prior work has also used scatterometer data together with multiple in situ and remotely sensed data sources to compile TC size data for ROCI and several 10-m wind radii (e.g., Demuth et al. 2006; Landsea and Franklin 2013). These studies, however, may also have been negatively influenced by the heterogeneous sampling of the TC wind field. More recently, atmospheric reanalysis data has been used to compute TC size using the radius of the azimuthal-mean environmental pressure (Knaff and Zehr 2007). Finally, Knaff et al. (2014) constructed estimates of the radius in which the azimuthal-mean 850-hPa azimuthal wind equals 5 $m\,s^{-1}$ using infrared TC satellite data and reanalysis data to estimate TC size. However, both Knaff and Zehr (2007) and Knaff et al. (2014) may contain uncertainty due to the use of a climatological vortex decay rate to estimate TC size. Additionally, TC size estimates from Knaff et al. (2014) may also include uncertainty due to the use of a simple multiple linear regression equation when training infrared satellite imagery with reanalysis data to estimate TC size. Intercomparison of results from these studies is not straightforward given the heterogeneity of the various datasets used to calculate TC size and the use of differing TC size metrics that are not always strongly correlated (e.g., Liu and Chan 1999; Knaff et al. 2014; Chavas and Lin 2016). Moreover, these two issues have resulted in ambiguities in the definition of TC size given the use of several disparate TC size metrics that may sample different regions of the same TC.

In contrast to the input datasets used in prior TC size studies, the use of a fixed numerical weather prediction model and data assimilation system in reanalyses (e.g., Thorne and Vose 2010; Bosilovich et al. 2013; Parker 2016) provides an opportunity for constructing a multidecadal TC size dataset that homogeneously samples each TC in space and time. However, there are three possible caveats when estimating TC size using reanalyses, including 1) TCs being too weak to define an outer TC size due to the coarse horizontal grid spacing and conservative physics parameterizations in reanalyses (e.g., Schenkel and Hart 2012; Murakami 2014; Hodges et al. 2017), 2) nonphysical trends in TC size due to changes in the observing system in time and space (e.g., Manning and Hart 2007; Thorne and Vose 2010; Bosilovich et al. 2013; Parker 2016), and 3) nonphysical TC structure due to the inability of reanalyses to resolve the TC inner core or due to reanalysis coding errors (Schenkel and Hart 2012; Murakami 2014; Kobayashi et al. 2015; Hodges et al. 2017). The impact of these potential caveats on reanalysis TC size has yet to be evaluated as previous work has primarily focused on examining the fidelity of reanalysis TC position, intensity, and thermodynamic structure (e.g., Manning and Hart 2007; Schenkel and Hart 2012; Murakami 2014; Wood and Ritchie 2014; Hodges et al. 2017).

Unauthenticated | Downloaded 01/17/23 09:26 PM UTC

Despite not focusing on reanalysis TC size, previous work has identified three parameters that serve as proxies for other factors that may influence the fidelity of reanalysis TC representation: 1) best-track TC latitude, 2) extended best-track TC size (Demuth et al. 2006), and 3) best-track TC age (i.e., time that has elapsed since best-track TC maximum 10-m wind speed first equals or exceeds 34 kt (17 m s^{-1}); Kossin et al. 2007a,b; Schenkel and Hart 2012). Specifically, reanalysis TC intensity was found to increase with increasing latitude (Schenkel and Hart 2012), which was a nonphysical artifact of reanalyses potentially resulting from greater observation densities at higher latitudes (Hatsushika et al. 2006; Vecchi and Knutson 2008), increasing postprocessed grid spacing with increasing latitude (Schenkel and Hart 2012), and weaker, more easily resolvable horizontal gradients associated with the expansion of the TC wind field in extratropically transitioning TCs (e.g., Brand and Guard 1979; Hart et al. 2006; Evans and Hart 2008). Second, reanalysis TC intensity exhibited systematic increases with larger extended best-track TC sizes potentially due to weaker, more easily resolvable horizontal gradients in larger TCs and an increased number of observations sampling these larger TC wind fields (Schenkel and Hart 2012). Third, TC age was also shown to be positively correlated with reanalysis TC intensity, which was also hypothesized to be a nonphysical reanalysis artifact possibly resulting from older TCs being better sampled by observations with time and the inability of reanalyses to simulate realistic TC intensification processes (Schenkel and Hart 2012). Each of these three factors are also likely strongly correlated with one another (Schenkel and Hart 2012).

It is important to note that reanalyses have been previously used for several TC-related applications including using reanalysis TC winds to derive TC size datasets (Knaff and Zehr 2007; Knaff et al. 2014) and calculating TC power dissipation (Sriver and Huber 2006). Reanalysis thermodynamic fields have been used to diagnose the onset and end of extratropical transition for TCs (e.g., Evans and Hart 2003; Kitabatake 2011; Wood and Ritchie 2014). Reanalysis wind and thermodynamic fields have also been used to identify potentially "missing" TCs in observations prior to the satellite era (Truchelut and Hart 2011; Truchelut et al. 2013).

Given the advantages and disadvantages of reanalyses, the present study seeks to determine the fidelity of TC size for the outer near-surface wind field within four atmospheric reanalysis datasets through comparison with QuikSCAT data. Outer TC wind structure and size metrics are examined given their importance to the physics of the complete TC wind field (e.g., Chan and Chan 2014; Chavas and Emanuel 2014; Chan and Chan 2015b; Chavas et al. 2015; Chavas and Lin 2016) and the inability of reanalyses to resolve inner TC winds (Manning and Hart 2007; Schenkel and Hart 2012; Murakami 2014; Hodges et al. 2017). If proven accurate and precise, reanalyses potentially can provide a longer-term TC size dataset compared to QuikSCAT that more homogeneously samples the TC wind field in space and time. The present study has four main objectives: 1) analyze the accuracy and precision of reanalysis TC size and wind field structure relative to observations, 2) investigate whether an optimal TC size metric exists in each reanalysis dataset, 3) determine which reanalysis dataset has TC size and structure estimates that most closely match observations, and 4) examine the fidelity of reanalysis TC size beyond the QuikSCAT era (2000–09). The applications of these results include, but are not limited to, using reanalysis-derived TC size estimates to construct radial profiles of azimuthal-mean near-surface winds (Chavas et al. 2015; Chavas and Lin 2016) for use in wind and storm surge modeling (Lin et al. 2014; Lin and Emanuel 2016).

For the remainder of the manuscript, section 2 describes the datasets used as well as the methodology for computing TC size. Section 3a intercompares the precision and accuracy of reanalysis TC size with QuikSCAT, while section 3b examines the full radial profile of TC winds. Section 3c analyzes the potential relationships of reanalysis TC size with parameters such as TC latitude and observed TC size. Section 3d investigates reanalysis TC size estimates throughout the QuikSCAT and satellite eras, when QuikSCAT TC size data are not always available. Section 4 summarizes the results.

2. Data and methods

a. Data

1) Reanalysis data

In the present study, the fidelity of TC size is examined within four atmospheric reanalysis datasets: 1) the National Centers for Environmental Prediction (NCEP) Climate Forecast System Reanalysis (CFSR; Saha et al. 2010), 2) the European Centre for Medium-Range Weather Forecasts (ECMWF) interim reanalysis (ERA-Interim, hereafter ERA-I; Dee et al. 2011), 3) the Japanese Meteorological Agency (JMA) Japanese 55-year Reanalysis (JRA-55; Kobayashi et al. 2015), and 4) the National Aeronautics and Space Administration (NASA) Modern-Era Retrospective Analysis for Research and Applications, version 2 (MERRA-2; Gelaro et al. 2017). The salient details for each reanalysis are provided in Table 1.

As shown in Table 1, three of the four reanalyses supplement TC initialization at each analysis time to

Unauthenticated | Downloaded 01/17/23 09:26 PM UTC

TABLE 1. Information on the four reanalyses datasets used in this study. For the number denoting the native reanalysis grid spacing, T refers to the mean wave truncation number, C refers to the number of points across each model tile for a cubed sphere grid, and L refers to the number of vertical levels. The asterisk denotes the approximate horizontal grid spacing for the postprocessed data for reduced Gaussian grids.

Dataset	Native grid spacing	Postprocessed grid spacing	Radial profile grid spacing (km)	Reanalysis period	TC initialization	Reference
NCEP CFSR	T382 L64	0.50° × 0.50°L37	27.5	1979–2010	Vortex relocation	Saha et al. (2010)
ECMWF ERA-I	T255 L60	0.70° × 0.70°* L37	37.5	1979–2015	None	Dee et al. (2011)
JMA JRA-55	T319 L60	0.56° × 0.56°* L60	30.0	1979–2015	TC wind profile retrieval	Kobayashi et al. (2015)
NASA MERRA-2	C180 L72	0.625° × 0.50° L42	32.5	1980–2015	Vortex relocation	Gelaro et al. (2017)

improve TC representation (e.g., Hatsushika et al. 2006; Schenkel and Hart 2012; Murakami 2014; Hodges et al. 2017). Specifically, the JRA-55 utilizes TC wind profile retrievals, which involves the assimilation of synthetic dropwindsondes created from an approximation of the TC wind field that incorporates best-track TC intensity and size data (Hatsushika et al. 2006; Onogi et al. 2007; Kobayashi et al. 2015). The use of TC wind profile retrievals has been shown to minimize reanalysis TC position errors and improve the representation of reanalysis TC intensity and structure (e.g., Schenkel and Hart 2012; Murakami 2014; Kobayashi et al. 2015; Hodges et al. 2017). It is important to note that the wind speed of the synthetic dropwindsondes in the JRA-55 exhibits a nonphysical weakening trend beginning in 1988 resulting in decreasing TC detection rates and weaker than expected TC structure (Kobayashi et al. 2015). The CFSR and MERRA-2 utilize vortex relocation, which involves either 1) relocating the reanalysis TC to its best-track location at each analysis time or 2) inserting a bogus vortex if the reanalysis TC is missing or too weak (Liu et al. 2000; Saha et al. 2010; Gelaro et al. 2017). In addition to reducing reanalysis TC position errors, the relocation of the TC may also improve the estimation of TC intensity and structure, potentially due to the improved representation of TC–environment interactions and a heightened probability of near-TC observations being assimilated by the reanalysis (e.g., Saha et al. 2010; Schenkel and Hart 2012; Murakami 2014; Hodges et al. 2017). However, a coding error in the vortex relocation for the CFSR has resulted in the occurrence of nonphysical TC structure in some cases (Schenkel and Hart 2012).

2) QUIKSCAT DATA

To compare reanalysis TC size with observations, we use version 1 of the QuikSCAT Tropical Cyclone Radial Structure Dataset (QSCAT-R; Chavas and Vigh 2014). QSCAT-R provides radial profiles of the azimuthal-mean 10-m azimuthal wind calculated from version 3 of the NASA Jet Propulsion Laboratory (JPL) QuikSCAT database that has been further optimized for TCs using a neural network algorithm to increase its accuracy and reduce rain contamination (Stiles et al. 2014). QSCAT-R provides radial wind profiles for selected TCs globally from 2000 to 2009 with a horizontal grid spacing of 6.25 km accurately measuring wind speeds up to 40 m s^{-1} (Chavas and Vigh 2014).

It is important to note that QuikSCAT data are ingested and assimilated into each reanalysis suggesting that reanalysis and QSCAT-R TC size are not necessarily independent. Assimilation of QuikSCAT data likely improves reanalysis TC size estimates at the nearest 6-h time to the QuikSCAT overpass and potentially beyond owing to the improved representation of TC–environment interactions in reanalyses. Moreover, TC representation both before and after the QuikSCAT overpass is also likely improved in the ERA-I and JRA-55 owing to the use of four-dimensional variational data assimilation (Dee et al. 2011; Kobayashi et al. 2015).

Despite the lack of independence between QuikSCAT and reanalyses, there are five reasons why reanalysis and QSCAT-R TC size may differ: 1) QuikSCAT and, thus, QSCAT-R sample the TC wind field in 1800-km swaths that may miss part of the TC wind field, 2) QuikSCAT cannot retrieve wind data in regions of rainfall (e.g., Stiles et al. 2014), 3) the horizontal grid spacing of QSCAT-R is a factor of ~4–6 times finer than reanalyses (Table 1), 4) reanalyses ingest QuikSCAT data at a coarsened horizontal grid spacing that may exclude data near the swath edges (e.g., data coarsened to 50-km horizontal grid spacing; Dee et al. 2011), and 5) reanalyses are numerical weather prediction models that may contain strong differences with observed TC structure and position (e.g., Schenkel and Hart 2012; Murakami 2014; Hodges et al. 2017) such that QuikSCAT data ingested by the reanalysis have negligible impact.

3) BEST-TRACK TC DATA

The present analysis examines North Atlantic (NA) and western North Pacific (WNP) TCs from version 3, revision 9, of the International Best Track Archive for Climate Stewardship (IBTrACS; Knapp et al. 2010).

Unauthenticated | Downloaded 01/17/23 09:26 PM UTC

Specifically, National Hurricane Center data are used for NA TCs and Joint Typhoon Warning Center data are utilized for WNP TCs. NA and WNP TCs are chosen for analysis given that these basins contain the smallest errors in reanalysis TC track and intensity (e.g., Schenkel and Hart 2012; Murakami 2014) and to avoid the greater uncertainty of IBTrACS data for north Indian Ocean and Southern Hemisphere TCs (e.g., Landsea et al. 2006).

In light of the reanalysis TC position errors (Schenkel and Hart 2012; Hodges et al. 2017), reanalysis TC position is determined in three steps (Brammer 2017). To begin, the first-guess position for the reanalysis TC is defined using the IBTrACS position added to the previous 6-h vector difference between the reanalysis and IBTrACS TC location. Next, the center of mass near the first-guess position is computed for six reanalysis variables: mean sea level pressure, 925-hPa relative vorticity, 850-hPa relative vorticity, 700-hPa relative vorticity, 850-hPa geopotential height, and 700-hPa geopotential height (Marchok 2002). Finally, reanalysis TC position is defined by averaging the centers of mass from the six reanalysis variables that are found within 300 km of the 850-hPa relative vorticity center of mass (Brammer 2017). Use of alternative TC recentering methods (Nguyen et al. 2014; Ryglicki and Hart 2015; Ryglicki and Hodyss 2016) do not significantly alter the results. It is important to emphasize that this methodology is not a TC tracker, which is largely independent from the IBTrACS tracks (Schenkel and Hart 2012; Murakami 2014; Hodges et al. 2017). Rather our methodology is strongly dependent on the IBTrACS by using each 6-h IBTrACS position as a first guess to help locate the corresponding reanalysis TC position.

In the current study, we first examine TCs of at least tropical storm strength (best-track 1-min maximum 10-m wind speed $\geq 17.5\,\mathrm{m\,s^{-1}}$) that are sampled by QSCAT-R before investigating TCs throughout the QSCAT-R era (2000–09) and satellite era (~1979–2015; see Table 1 for reanalysis availability). Given that QSCAT-R does not necessarily correspond to regular synoptic times, best-track data are interpolated to the time of the QSCAT-R overpass using linear interpolation.

b. Methodology for calculating TC size

In the present study, TC size is defined as the size of outer near-surface azimuthal wind field. Six outer TC size metrics are examined including the radius at which the azimuthal-mean 10-m azimuthal wind equals 2 (r_2), 4 (r_4), 6 (r_6), 8 (r_8), 10 (r_{10}), and $12\,\mathrm{m\,s^{-1}}$ (r_{12}). Similar outer TC size metrics have been used in prior work (e.g., Chavas and Emanuel 2010; Knaff et al. 2014; Chavas and Lin 2016), which partially motivates examining a range of thresholds. Most importantly, the azimuthal wind speed threshold yielding the closest match between reanalyses and QSCAT-R is of great interest for developing a reanalysis TC size dataset.

In the present study, reanalysis TC size is defined using the azimuthal-mean 10-m azimuthal wind following Chavas and Vigh (2014):

1) construct a TC-centered polar coordinate system for 10-m total wind vectors at the postprocessed grid spacing of each dataset (Table 1);
2) exclude all 10-m total wind vectors over land;
3) remove the environmental wind field, which is assumed to be uniform at all radii and is empirically defined as the TC translation vector rotated 20° cyclonically and reduced by a factor of 0.55 (Lin and Chavas 2012);
4) compute the azimuthal wind field and calculate the azimuthal-mean wind profile;
5) interpolate the radial profile of the azimuthal-mean 10-m azimuthal wind to a regular grid with grid spacing equivalent to ~0.5 times the horizontal grid spacing of each dataset (Table 1) using a piecewise cubic Hermite interpolating polynomial;
6) remove all radial data points where the data asymmetry parameter χ is greater than 0.5, where χ is defined as the magnitude of the vector mean of all vectors from the storm center to each defined grid point included at a given radius normalized by the mean distance of the storm center to each grid point (Chavas and Vigh 2014);
7) extract r_2, r_4, r_6, r_8, r_{10}, and r_{12} from the radial profile of the azimuthal-mean 10-m azimuthal wind; and
8) exclude any TC size estimates if any of the following three conditions are met for both QSCAT-R and reanalyses: (i) TC size estimate is less than 50 km (i.e., ~4 times QuikSCAT horizontal grid spacing; Chavas et al. 2016), (ii) radial profiles of azimuthal-mean 10-m azimuthal wind radially inwards of the reanalysis TC size estimate contain missing data over two or more consecutive reanalysis radial grid points or over the equivalent radial distance in QSCAT-R, or (iii) reanalysis or QSCAT-R TC size is undefined.

As an example of case studies with precise and imprecise TC size estimates, Figs. 1a,b contain radial profiles of the azimuthal-mean 10-m azimuthal wind for NA TC Isabel at 1028 UTC 15 September 2003 and NA TC Epsilon at 2058 UTC 05 December 2005, respectively. Figure 1a shows that both the shape and magnitude of TC Isabel's outer reanalysis wind field is in close agreement with QSCAT-R, especially at radii beyond 300 km. As a result, reanalysis r_8 is very close to QSCAT-R r_8 with differences ranging from ~3 to 34 km. It is important to emphasize that TC size is

Unauthenticated | Downloaded 01/17/23 09:26 PM UTC

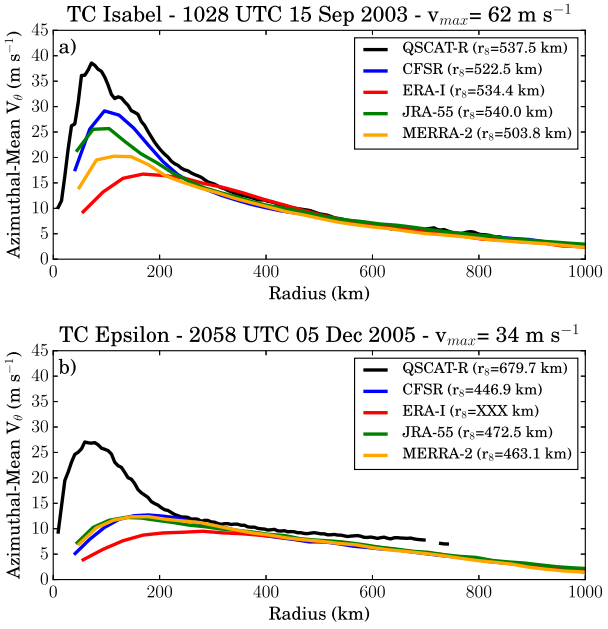

FIG. 1. Radial profile of azimuthal-mean 10-m azimuthal wind (m s^{-1}) from QSCAT-R, CFSR, ERA-I, JRA-55, and MERRA-2 for (a) TC Isabel at 1028 UTC 15 Sep 2003 and (b) TC Epsilon at 2058 UTC 05 Dec 2005. The r_8 (km) is provided in the legend for each dataset; r_8 is not defined for TC Epsilon in the ERA-I.

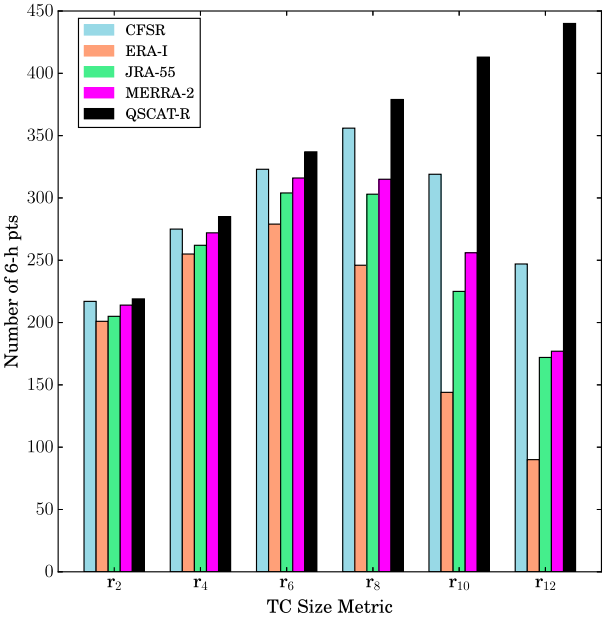

FIG. 2. Number of 6-h QSCAT-R and corresponding reanalysis data points for r_2, r_4, r_6, r_8, r_{10}, and r_{12} in the NA.

accurately measured despite the underestimation of the wind field near the TC center, which occurs for many reanalysis TCs (e.g., Schenkel and Hart 2012; Murakami 2014; Kobayashi et al. 2015; Hodges et al. 2017). In contrast, Fig. 1b shows large differences in the shape and magnitude of the outer wind field of TC Epsilon between reanalyses and QSCAT-R, as the storm is weakly represented in reanalyses. As expected, differences between reanalysis and QSCAT-R r_8 for TC Epsilon are large ranging from ~207 to 233 km with the ERA-I wind field being too weak to estimate r_8. As will be shown below, the majority of TCs are represented in a manner that generally falls between these two cases.

c. *Statistical significance testing*

The present study utilizes three types of statistical significance testing. Statistical comparison of median values is conducted using the 95% confidence interval of medians computed from a 1000-sample bootstrap approach with replacement for a two-tailed test. The statistical difference of Pearson correlation coefficients from zero is determined by computing its 95% confidence interval for a two-tailed test using a Fisher transformation. Finally, the statistical similarities between TC size distributions are determined using two-sample Kolmogorov–Smirnov testing at the 5% level for a two-tailed test. The number of distinctly named TCs, rather than the number of 6-h IBTrACS data points, is conservatively chosen as the sample size used in the 1000-sample bootstrap approach and in the Fisher transformation (e.g., Schenkel and Hart 2012, 2015a,b) given the stability in time of the outer circulation for each TC (e.g., Weatherford and Gray 1988a; Merrill 1984; Chavas and Emanuel 2010; Chavas and Lin 2016).

3. Analysis and results

a. *Quantifying the precision and accuracy of reanalysis TC size*

The analysis begins by examining all QSCAT-R TC size observations for each TC size metric to determine how often a corresponding reanalysis TC size can be estimated for the NA (Fig. 2) and WNP (Fig. 3). Reanalysis r_2, r_4, r_6, and r_8 are defined for a substantial majority of QSCAT-R TC size estimates ~65%–99% regardless of the basin or reanalysis examined. In contrast, reanalysis r_{10} and r_{12} are defined for a smaller percentage of QSCAT-R TC size estimates ~20%–78% largely due to reanalyses frequently being unable to resolve azimuthal-mean 10-m azimuthal wind speeds at or exceeding ~10 m s^{-1}, especially in the NA (e.g., Schenkel and Hart 2012; Murakami 2014; Hodges et al. 2017). Comparison of NA and WNP TCs reveals that reanalysis TC size is defined for a greater fraction of WNP cases. Intercomparison among reanalyses reveals that TC size is

Unauthenticated | Downloaded 01/17/23 09:26 PM UTC

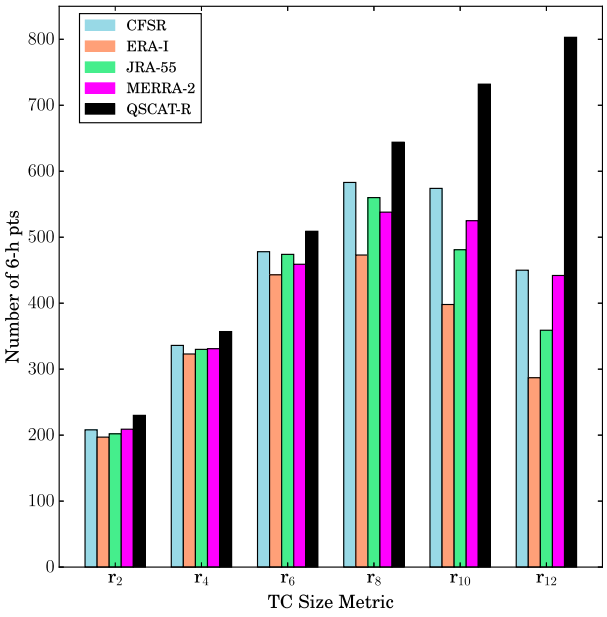

FIG. 3. As in Fig. 2, but for WNP TCs.

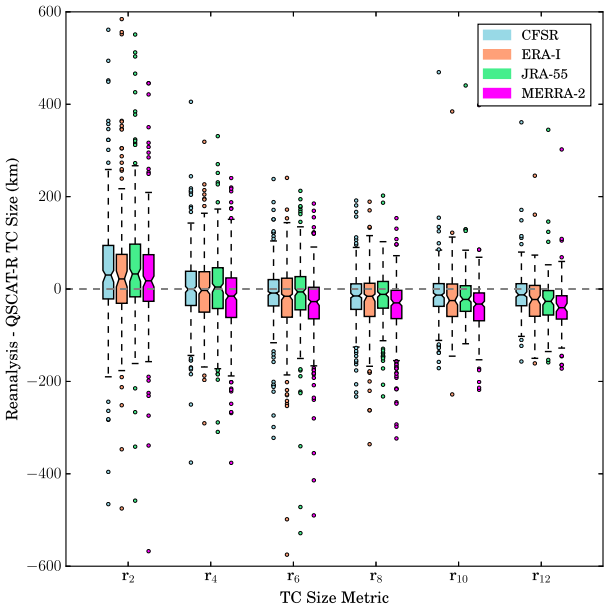

FIG. 4. Box-and-whisker plots for the difference between reanalysis and QSCAT-R (along the x axis) r_2, r_4, r_6, r_8, r_{10}, and r_{12} (km) in the NA. The box plot displays the median (black horizontal line near box center), the 95% confidence interval of the median calculated from a 1000-sample bootstrap approach with replacement (notches on boxes), the interquartile range (box perimeter; $[q_1, q_3]$), whiskers {black dashed; $[q_1 - 1.5(q_3 - q_1), q_3 + 1.5(q_3 - q_1)]$}, and outliers (filled circles).

defined more frequently in the JRA-55, MERRA-2, and especially the CFSR compared to the ERA-I likely because of improved reanalysis TC representation resulting from their use of either vortex relocation or TC wind profile retrievals (Table 1; e.g., Schenkel and Hart 2012; Murakami 2014; Hodges et al. 2017).

With these results in mind, the remainder of the analysis, with the exception of section 3d, only compares cases where both QSCAT-R and reanalysis TC size are defined for a given TC size metric. To quantify the precision of reanalysis TC size estimates, box-and-whisker plots of the difference between reanalysis and QSCAT-R TC size are shown for each TC size metric in the NA (Fig. 4) and WNP (Fig. 5). Regardless of the basin and TC size metric examined, reanalysis TC size is generally comparable to QSCAT-R as evidenced by median TC size differences ranging between −71 and 50 km, which is approximately less than or equal to one reanalysis grid point (Table 1). Relative to the magnitude of QSCAT-R TC size, the median TC size difference between reanalyses and QSCAT-R ranges between 6% and 18%. Moreover, TC size differences become increasingly negative with increasingly narrower distributions when transitioning from r_2 to r_{12} in both basins such that r_2 is larger and r_{12} is smaller in reanalyses than in QSCAT-R. NA TC size differences are generally less biased for all TC size metrics compared to WNP TCs as evidenced by narrower distributions and smaller median differences. Finally, the CFSR and JRA-55 generally have the smallest median TC size differences and narrowest distributions for most TC size metrics in each basin, suggestive of the importance of vortex relocation and TC wind profile retrievals. However, MERRA-2 exhibits the largest TC size differences despite the use of vortex relocation suggesting

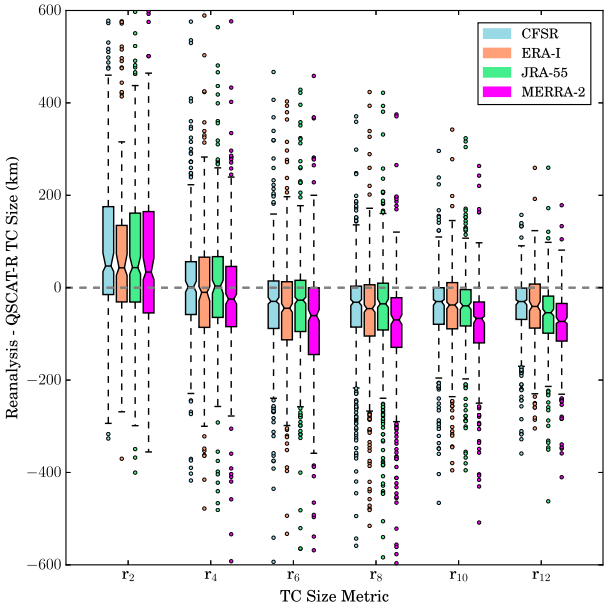

FIG. 5. As in Fig. 4, but for WNP TCs.

Unauthenticated | Downloaded 01/17/23 09:26 PM UTC

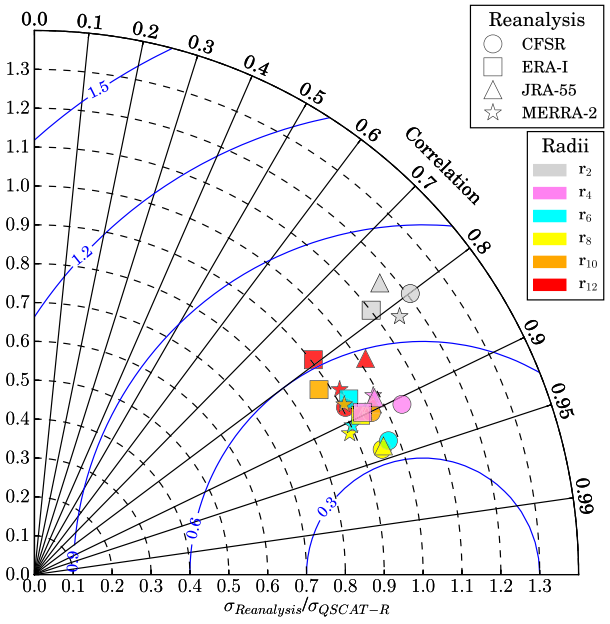

FIG. 6. Taylor diagram depicting the Pearson correlation coefficients (black solid lines), normalized standard deviations (black dashed lines), and root-mean-square difference (solid blue lines) between r_2, r_4, r_6, r_8, r_{10}, and r_{12} (represented by different colors) from QSCAT-R and each of the four reanalyses. All Pearson correlation coefficients are statistically significantly different from 0 at the 95% confidence interval for a two-tailed test ($p \ll 0.05$).

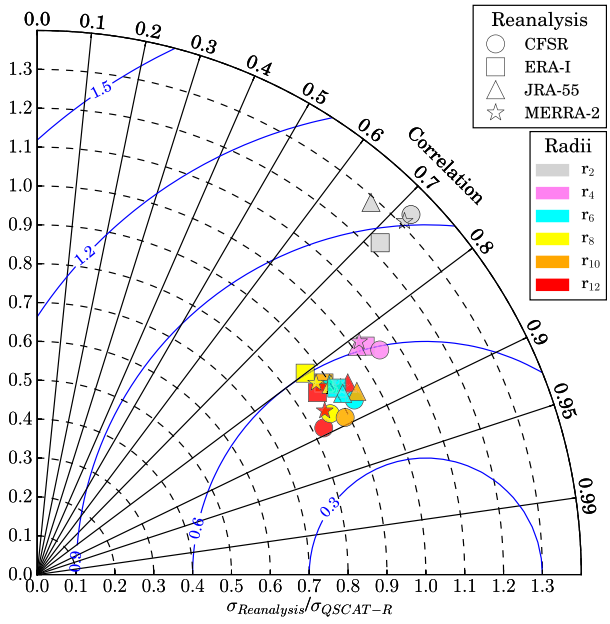

FIG. 7. As in Fig. 6, but for WNP TCs.

the importance of other factors (e.g., model numerics and physics; Reed and Jablonowski 2011, 2012; Reed et al. 2012) in reanalysis TC size representation.

The accuracy of reanalysis TC size relative to QSCAT-R is depicted in Taylor diagrams containing the Pearson correlation coefficients, normalized standard deviations, and root-mean-square difference calculated between QSCAT-R and each reanalysis for all TC size metrics in the NA (Fig. 6) and WNP (Fig. 7). Figures 6 and 7 reveal strong, statistically significant correlations ($0.62 \le R \le 0.94; p < 0.05$) for all TC size metrics in each reanalysis in the NA and WNP. The vast majority of normalized standard deviations in Figs. 6 and 7 ($0.83 \le \sigma_{\text{reanalysis}}/\sigma_{\text{QSCAT–R}} \le 1.29$) are generally close to, but less than 1, indicating that the variability in reanalysis TC size is less than QSCAT-R. Of all TC size metrics, r_8 exhibits the strongest correlations ($0.89 \le R \le 0.94; p \ll 0.05$) with normalized standard deviations closest to 1 ($0.90 \le \sigma_{\text{reanalysis}}/\sigma_{\text{QSCAT–R}} \le 0.96$) in the NA for all reanalyses, while either r_6 ($0.83 \le R \le 0.88; p \ll 0.05; 0.89 \le \sigma_{\text{reanalysis}}/\sigma_{\text{QSCAT–R}} \le 0.93$) or r_{10} ($0.83 \le R \le 0.89; p \ll 0.05; 0.88 \le \sigma_{\text{reanalysis}}/\sigma_{\text{QSCAT–R}} \le 0.95$) are most comparable between WNP reanalysis and QSCAT-R TCs. In both the NA and WNP, r_2 ($0.62 \le R \le 0.82; p < 0.05; 1.11 \le \sigma_{\text{reanalysis}}/\sigma_{\text{QSCAT–R}} \le 1.29$) is particularly poorly represented, likely due to the difficulty in separating the TC wind field from background noise at weak wind speed thresholds (Chavas and Emanuel 2010; Chavas and Vigh 2014; Chavas and Lin 2016). Relative to the WNP, NA TCs generally exhibit stronger correlations with normalized standard deviations closer to 1. When comparing individual reanalyses, both the CFSR and JRA-55 generally most closely match QSCAT-R TC size as expected given the supplemental TC initialization used in these datasets.

Together, the results presented thus far yield the following broader conclusions regarding reanalysis TC size:

- The high precision and accuracy of TC size metrics, especially r_6–r_{10}, in both basins suggest that outer TC structure is well represented in reanalyses.
- Radii r_6–r_8 in the NA and r_6–r_{10} in the WNP are generally the optimal TC size metrics to examine in each basin given the percentage of defined reanalysis TC size estimates and their precision and accuracy relative to QSCAT-R TC size.
- NA TC size is represented with greater accuracy and precision than WNP TC size in reanalyses.
- The CFSR and JRA-55 are the reanalyses that most closely match QSCAT-R TC size, suggesting the importance of supplementing TC initialization with either vortex relocation or TC wind profile retrievals.

b. *Analysis of the radial profile of TC winds*

To supplement the prior results on TC size, the median (solid line) with its 95% confidence interval

Unauthenticated | Downloaded 01/17/23 09:26 PM UTC

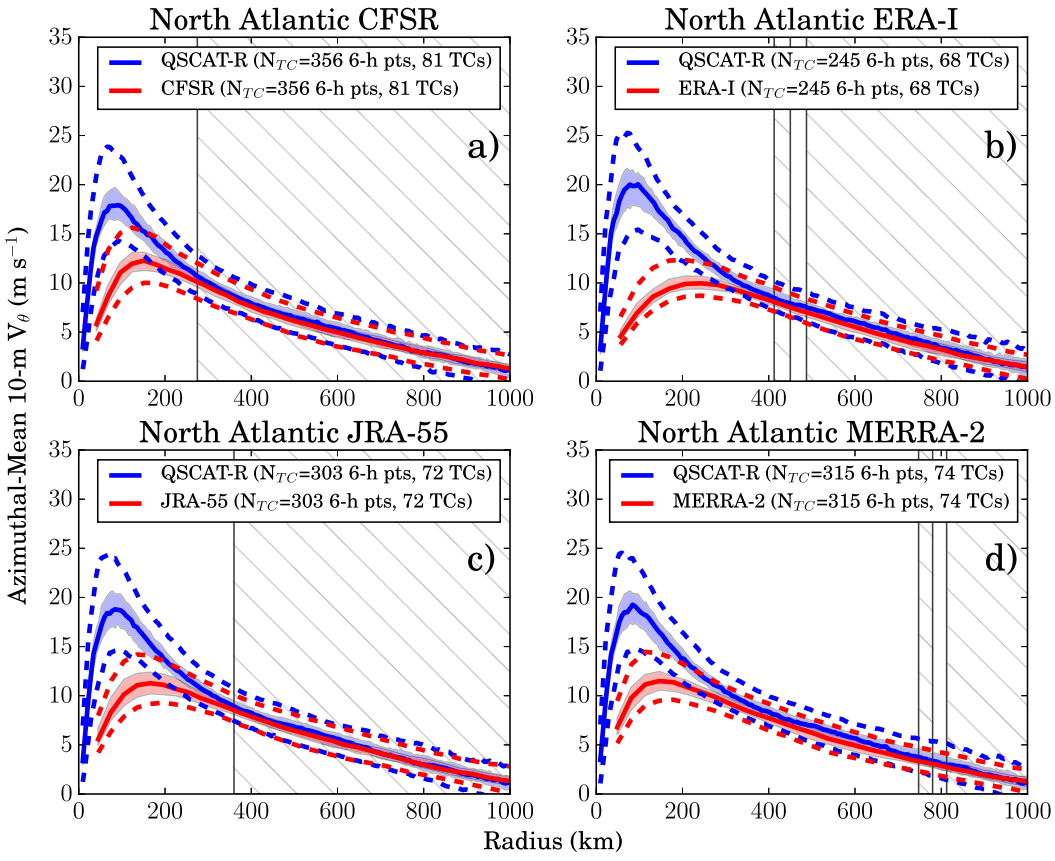

FIG. 8. Median (solid lines) with their 95% confidence interval calculated from a 1000-sample bootstrap approach with replacement (shading) and the interquartile range (dashed lines) for the radial profile of the azimuthal-mean 10-m azimuthal wind (m s^{-1}) in QSCAT-R and the (a) CFSR, (b) ERA-I, (c) JRA-55, and (d) MERRA-2 for NA TCs. The hatched background denotes radii at which the distribution of QSCAT-R and reanalysis wind values are likely taken from the same parent distribution as determined from a two-sample Kolmogorov–Smirnov test ($p > 0.05$).

(shading) and the interquartile range (dashed lines) for the radial profile of the azimuthal-mean 10-m azimuthal wind in QSCAT-R and each reanalysis are featured for NA (Fig. 8) and WNP TCs (Fig. 9). The hatched background denotes radii in which the distributions of reanalysis and QSCAT-R TC winds are likely not statistically significantly different according to a two-sample Kolmogorov–Smirnov test ($p > 0.05$). Figures 8 and 9 demonstrate that reanalysis TC winds, especially in the WNP, are generally weaker than QSCAT-R, consistent with reanalysis r_6–r_{12} largely being smaller than QSCAT-R (Figs. 4 and 5). In fact, neither the lower quartile nor, in some reanalyses, the median wind speed exceed 12 m s^{-1} in the WNP and 10 m s^{-1} in the NA at any radii. Such a result explains why r_{12} in the WNP and NA and r_{10} in the NA are frequently undefined in reanalyses (Figs. 2 and 3). NA TCs in the CFSR, ERA-I, and JRA-55 have wind distributions that are not statistically significantly different from QSCAT-R beginning at radii greater than or equal to 289, 431, and 375 km, respectively. These radial distances are ~5–7 times the native model grid spacing in the CFSR, ERA-I, and JRA-55, consistent with the effective horizontal grid spacing in other models (e.g., Skamarock 2004), potentially providing a minimum horizontal scale for using reanalyses to examine various phenomena. Comparison of Figs. 8 and 9 with Figs. 2 and 3 reveals that r_2–r_8 are generally located at radii beyond ~5–7 times the reanalysis grid spacing, explaining why these TC size radii are generally regularly defined. Compared to the NA, WNP reanalysis TC winds are more strongly, and significantly, underestimated compared to QSCAT-R at all radii within all reanalyses (Fig. 9). This result is consistent with the larger differences between reanalysis and QSCAT-R TC size in the WNP (Fig. 5). Despite the low bias in WNP reanalysis TC winds, the width of the interquartile range and shape of the radial profile of reanalysis and QSCAT-R wind fields are very similar especially at and radially outward of ~300–400-km radius (~5–7 times the native model grid spacing)

Unauthenticated | Downloaded 01/17/23 09:26 PM UTC

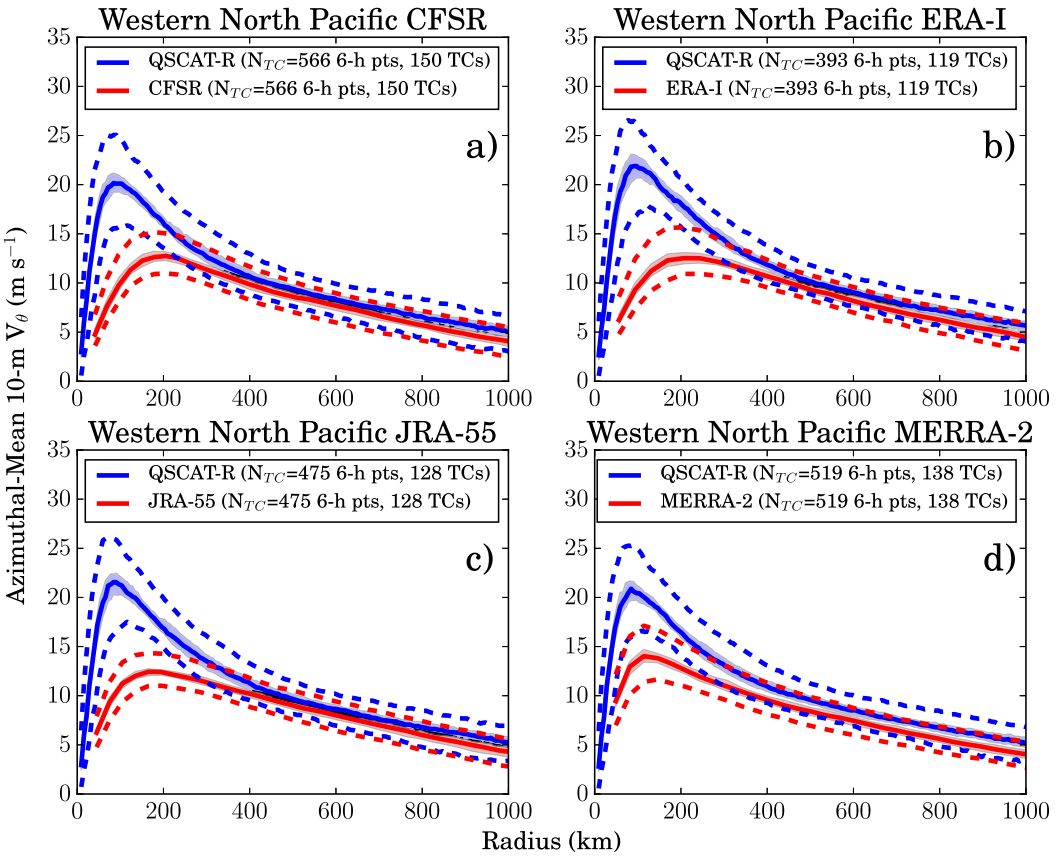

FIG. 9. As in Fig. 8, but for WNP TCs.

providing some confidence that reanalyses can also reasonably represent TC structure.

Additional insight is obtained by examining joint histograms of the azimuthal-mean 10-m azimuthal wind for NA (Fig. 10) and WNP (Fig. 11) TCs in QSCAT-R and each reanalysis. One-dimensional histograms of QSCAT-R and reanalysis winds are located above and to the right, respectively, of the joint histograms. To compare the reanalysis and QSCAT-R winds on the same radial grid, QSCAT-R winds are interpolated to the horizontal grid spacing of each reanalysis using a piecewise cubic Hermite interpolating polynomial. Both Figs. 10 and 11 also include the Pearson correlation coefficients calculated between reanalysis and QSCAT-R winds in each joint histogram. The joint histograms and their respective correlations ($0.77 \leq R_{\text{all}} \leq 0.89; p \ll 0.05$) suggest that the reanalysis and QSCAT-R wind fields are strongly correlated with small biases for QSCAT-R wind speeds less than or equal to 10 m s^{-1} ($0.80 \leq R_{\leq 10} \leq 0.93$; $p \ll 0.05$). However, reanalysis winds are strongly underestimated for QSCAT-R wind speeds greater than 10 m s^{-1} especially for the ERA-I in the NA ($R = 0.17$; $p > 0.05$), as well as in other reanalyses in both basins ($0.26 \leq R_{\leq 10} \leq 0.64$; $p < 0.05$) consistent with the underestimation of best-track TC intensity by reanalyses. Similar to the results for TC size, NA reanalysis TC winds generally exhibit stronger correlations with QSCAT-R than WNP TCs, especially for TC winds less than or equal to 10 m s^{-1}. While the CFSR, JRA-55, and MERRA-2 most closely match QSCAT-R for all wind speeds, the CFSR and JRA-55 consistently represent QSCAT-R TC wind speeds less than or equal to 10 m s^{-1} with the greatest fidelity, which agrees with the results for TC size (Figs. 4–7).

Consistent with the reanalysis TC size results, the azimuthal-mean 10-m azimuthal winds in reanalyses are similar to QSCAT-R particularly for wind speeds less than or equal to 10 m s^{-1}, providing insight into the strong correlations and small biases in outer TC size estimates, particularly for r_6–r_{10}. Most importantly, these results provide additional evidence suggesting that outer TC winds are well represented in reanalyses.

c. *Trends in the fidelity of reanalysis TC size*

The difference between reanalysis and QSCAT-R TC size exhibits trends with QSCAT-R TC size and TC

Unauthenticated | Downloaded 01/17/23 09:26 PM UTC

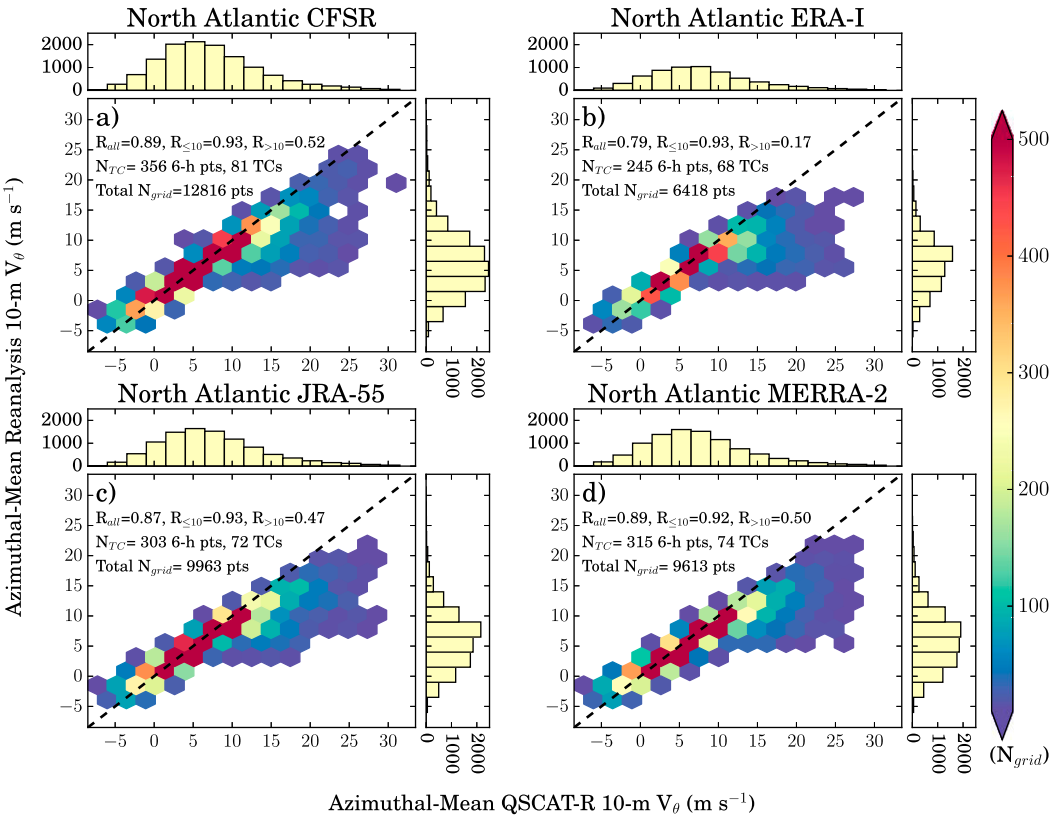

FIG. 10. Joint histogram (shaded hexagons) of the azimuthal-mean 10-m azimuthal wind (m s^{-1}) over the entire radial profile of TC winds for QSCAT-R and for the (a) CFSR, (b) ERA-I, (c) JRA-55, and (d) MERRA-2 in NA TCs. QSCAT-R winds have been interpolated to each respective reanalysis radial grid point using a piecewise cubic Hermite interpolating polynomial. The black dashed line denotes the 1:1 line where QSCAT-R and reanalysis winds have the same values. The histograms above and to the right of each figure denote the distributions of the azimuthal-mean 10-m azimuthal wind for QSCAT-R and each reanalysis, respectively. Pearson correlation coefficients for all grid points (R_{all}), grid points with QSCAT-R wind speeds ≤ 10 m s^{-1} ($R_{\leq 10}$), and grid points with QSCAT-R wind speeds > 10 m s^{-1} ($R_{>10}$) are listed. The number of 6-h IBTrACS data points and distinctly named TCs (N_{TC}) and the total number of radial grid points (Total N_{grid}) are provided for each dataset. All correlation coefficients are statistically significantly different from zero at the 95% confidence interval for a two-tailed test ($p \ll 0.05$), except for $R_{>10}$ for ERA-I NA TCs.

latitude. In the interest of brevity, the present section only examines r_8 in the NA and r_{10} in the WNP given that the trends for these TC size radii are similar to the other TC size metrics. Beginning with QSCAT-R TC size, box-and-whisker plots of the difference between reanalysis and QSCAT-R TC size and their sample sizes (shaded bars) are binned according to QSCAT-R r_8 in the NA (Fig. 12) and r_{10} in the WNP (Fig. 13). Figures 12 and 13 show that increasingly larger QSCAT-R TC size bins are associated with increasingly negative TC size differences with broader distributions, which is supported by moderate negative correlations between these two quantities ($-0.49 \leq R \leq -0.29$; $p < 0.05$). The increasing TC size differences for larger QSCAT-R TCs may be due to increased uncertainty in QSCAT-R TC size estimates given that outer TC radii are not always well sampled by the 1800-km QuikSCAT swath widths (Chavas and Emanuel 2010; Chavas and Vigh 2014; Chan and Chan 2015a; Chavas et al. 2016). This trend is particularly strong in the WNP compared to the NA perhaps because WNP TCs are generally larger than NA TCs (e.g., Merrill 1984; Liu and Chan 1999; Chavas and Emanuel 2010; Knaff et al. 2014).

With regard to the relationship between TC size differences and TC latitude, box-and-whisker plots of the difference between reanalysis and QSCAT-R TC size and their sample sizes (shaded bars) are binned according to TC latitude for WNP TCs (Fig. 14). A similar figure for NA TCs is not shown given the absence of a similar relationship between TC size and TC latitude in that basin ($-0.05 \geq R \geq 0.13$). Figure 14 reveals that WNP TCs in the ERA-I, JRA-55, and MERRA-2

Unauthenticated | Downloaded 01/17/23 09:26 PM UTC

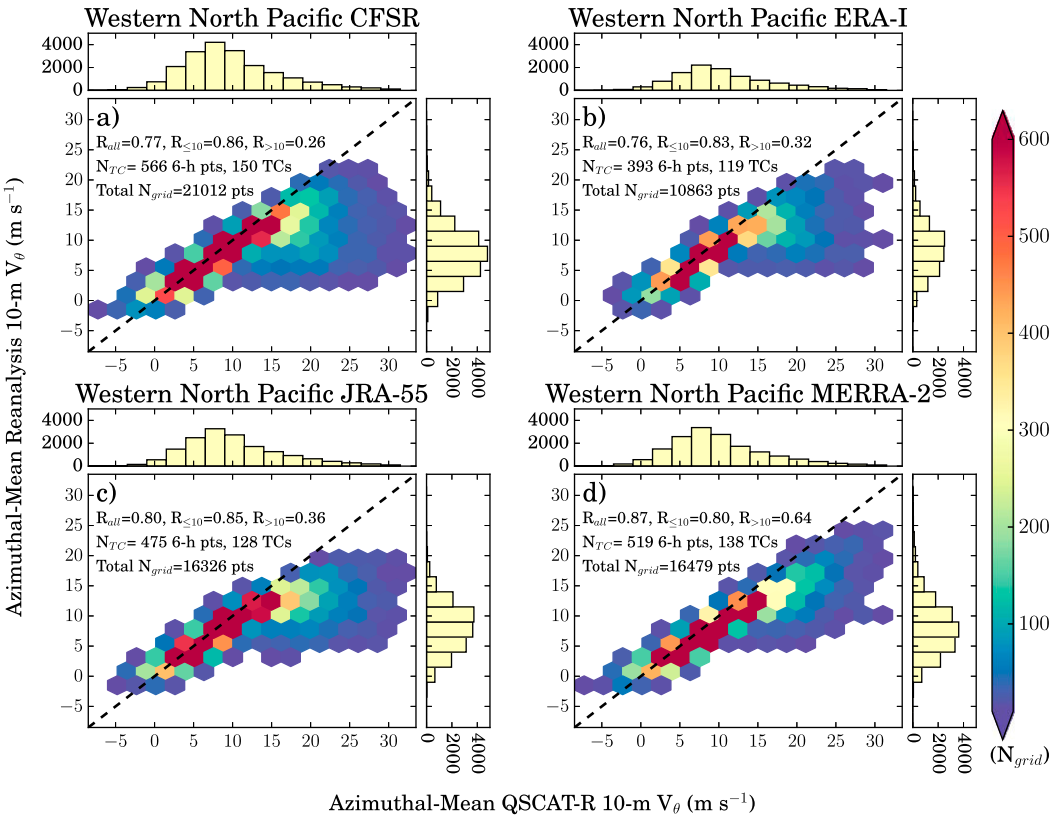

FIG. 11. As in Fig. 10, but for WNP TCs. Note the difference in the shading range in the joint histograms and the *y* axes in the one-dimensional histograms compared to Fig. 10.

exhibit decreasing TC size differences with increasing TC latitude as evidenced by decreasing median TC size differences with narrower distributions. These reanalyses exhibit weak yet significant correlations between TC size differences and TC latitude ($0.26 \leq R \leq 0.29$; $p < 0.05$). However, the source of these trends is unclear given the absence of similar trends for WNP TCs in the CFSR and NA TCs in all reanalyses.

These results suggest that reanalysis TC size, like reanalysis TC intensity, may be ascribed to both physical processes and nonphysical model artifacts (e.g., changes in observing system in space and time; Thorne and Vose 2010; Bosilovich et al. 2013; Parker 2016). Together, the relationships between TC size differences and both QSCAT-R TC size and TC latitude may imply that low-latitude, large WNP TC sizes may be particularly underestimated.

d. *Examining reanalysis TC size throughout QSCAT-R and satellite eras*

Given that outer TC size does not exhibit interdecadal trends (Knaff et al. 2014), reanalysis TC size distributions across different time periods (e.g., satellite era) should be comparable to QSCAT-R. With this in mind, the current results section compares distributions of reanalysis TC size for all 6-h IBTrACS TC data during the QSCAT-R era (2000–09) and during the satellite era (~1979–2015; Table 1) with the previously examined distribution of QSCAT-R TC size and the corresponding distribution of reanalysis TC size. Similar to the prior section, r_8 and r_{10} are used as TC size metrics in the NA and WNP, respectively, in the interest of brevity. Kernel density estimates and box-and-whisker plots for each of these four TC size subsets are featured for r_8 in the NA (Fig. 15) and r_{10} in the WNP (Fig. 16). It is important to note that the QSCAT-R TC size distribution (for r_{12}) has been previously shown to be lognormal (Chavas and Emanuel 2010; Chavas et al. 2016), which is used as a benchmark for evaluating the fidelity of reanalysis r_8 and r_{10} distributions.

Beginning by comparing QSCAT-R r_8 and r_{10} with the corresponding reanalysis r_8 and r_{10} values, Figs. 15 and 16 reveal that reanalysis r_8 in the NA and r_{10} in the WNP are qualitatively similar to the QSCAT-R distributions with positive skewness and approximately lognormal shape. In fact, Kolmogorov–Smirnov goodness-of-fit

Unauthenticated | Downloaded 01/17/23 09:26 PM UTC

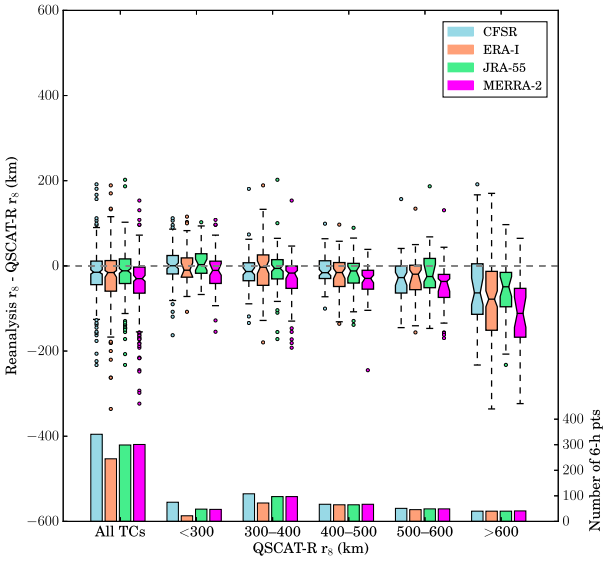

FIG. 12. Box-and-whisker plots for the difference between reanalysis and QSCAT-R r_8 (km; left y axis) binned according to QSCAT-R r_8 in the NA. The bar plots denote the number of 6-h TC size data points (N; right y axis) for each set of box and whiskers. See Fig. 4 for a description of the plotting conventions.

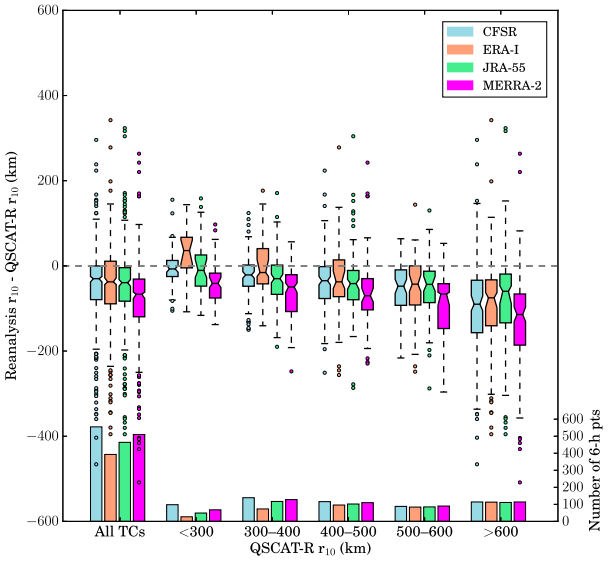

FIG. 13. As in Fig. 12, but binned by QSCAT-R r_{10} for WNP TCs. Note the difference in the y-axis range for the bar plots compared to Fig. 12.

testing ($p > 0.05$) reveals that the reanalysis r_8 and r_{10} distributions are likely lognormally distributed, except for the MERRA-2 in the NA. The distributions of both reanalysis r_8 and r_{10} are generally slightly biased toward smaller values with narrower distributions than QSCAT-R. In spite of these differences, the distributions of NA r_8 in the CFSR, ERA-I, and JRA-55 are likely similar to the corresponding distribution of QSCAT-R r_8 as suggested by two-sample Kolmogorov–Smirnov testing ($p > 0.31$) and median values that are not statistically significantly different from each other according to a 1000-sample bootstrap approach with replacement ($p > 0.05$; Figs. 15 and 16). In contrast, WNP r_{10} in QSCAT-R and each reanalysis are not similar as shown by two-sample Kolmogorov–Smirnov testing ($p \ll 0.01$) and statistically significantly different median TC values ($p < 0.05$; Figs. 15 and 16), likely due to the previously discussed underestimation of WNP TC winds in reanalyses (Figs. 9 and 11).

Examination of reanalysis r_8 and r_{10} distributions in the NA and WNP, respectively, for all 6-h IBTrACS data points during the QSCAT-R era and satellite era reveals similarities to the QSCAT-R distributions. Specifically, reanalysis r_8 and r_{10} distributions are approximately positively skewed with a lognormal shape, while exhibiting a similar width to QSCAT-R distributions. However, r_8 and r_{10} distributions during the QSCAT-R era and satellite era are not technically lognormal according to Kolmogorov–Smirnov goodness-of-fit tests ($p < 0.01$). Each reanalysis r_8 and r_{10} distribution during the QSCAT-R era and satellite era is also shifted toward smaller values in each basin relative to the QSCAT-R distribution with the exception of the ERA-I in the NA. Except for the JRA-55 in the NA during the satellite era ($p = 0.22$), none of the CFSR, JRA-55, or MERRA-2 r_8 and r_{10} distributions in the NA and WNP from either the QSCAT-R era or satellite era are statistically similar to QSCAT-R or the corresponding reanalysis distributions as revealed by two-sample Kolmogorov–Smirnov testing ($p < 0.02$). In contrast, two-sample Kolmogorov–Smirnov

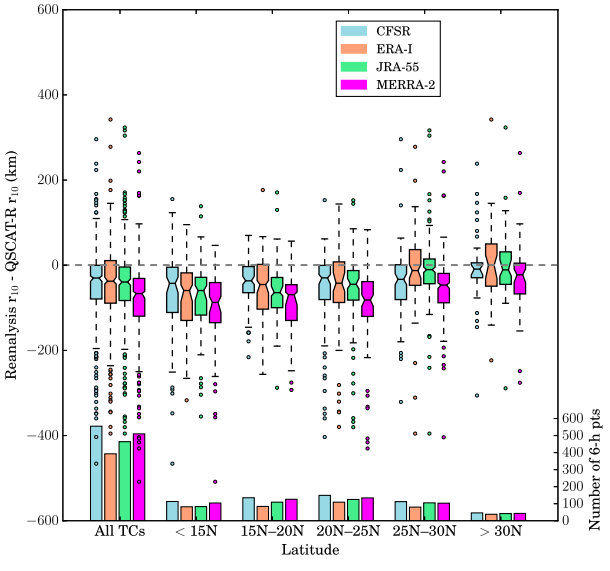

FIG. 14. As in Fig. 4, but binned by TC latitude for WNP TCs.

Unauthenticated | Downloaded 01/17/23 09:26 PM UTC

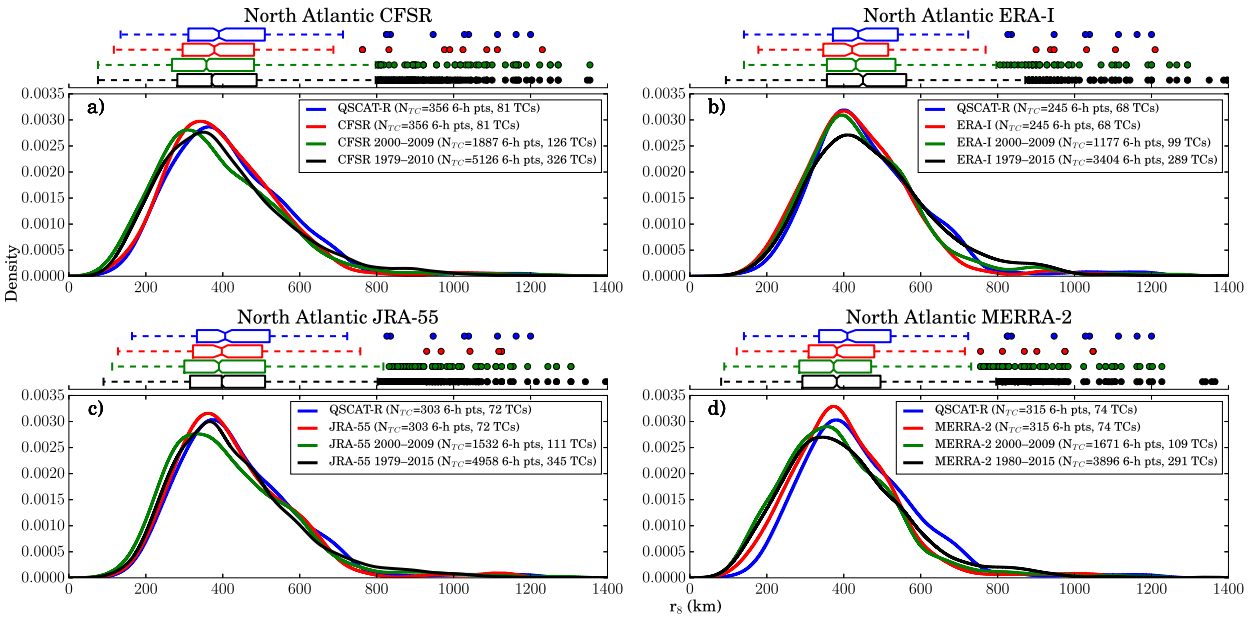

FIG. 15. Box and whiskers and kernel density estimate of NA r_8 (km) from QSCAT-R, reanalysis r_8 corresponding to the QSCAT-R r_8, all 6-h IBTrACS data points for reanalysis r_8 during the QSCAT-R era (2000–09), and all 6-h IBTrACS data points for reanalysis r_8 during the satellite era (1979–2015 for ERA-I and JRA-55; 1980–2015 for MERRA-2; 1979–2010 for CFSR) in the (a) CFSR, (b) ERA-I, (c) JRA-55, and (d) MERRA-2. The legend entries for each dataset contain the number of 6-h data points and distinctly named TCs (N_{TC}).

testing reveals that the ERA-I r_8 distributions in the NA during both the QSCAT-R era and satellite era are likely statistically similar to the QSCAT-R distribution ($p > 0.31$), while only the ERA-I r_{10} distribution in the WNP during the satellite era is likely statistically similar to the QSCAT-R distribution ($p = 0.11$).

These results for r_8 in the NA and r_{10} in the WNP suggest that reanalysis TC size distributions are generally well represented when the TC wind field is well sampled by QSCAT-R. Moreover, reanalysis TC size is represented with reasonable fidelity even when QuikSCAT data are not assimilated as is suggested by the analysis of the distributions of r_8 and r_{10} for all 6-h IBTrACS data points during the QuikSCAT era and satellite era. In addition to these results, there are several additional reasons to suggest that reanalysis TC size is generally well represented. Specifically, QuikSCAT sampled a small subset of TCs (e.g., 27% of NA TCs and 33% of WNP TCs; Chan and Chan 2012; Chavas and Vigh 2014; Chavas et al. 2016), which may not be representative of the entire TC size distribution, suggesting that discrepancies likely should exist between QSCAT-R TC sizes and either QSCAT-R era or satellite era TC sizes. Moreover, QuikSCAT observations are just one source of lower-tropospheric observations assimilated into reanalyses that may improve TC size representation (e.g., aircraft reconnaissance and ship and buoy data), which are available throughout the satellite era (e.g., Hatsushika et al. 2006; Saha et al. 2010; Dee et al. 2011; Kobayashi et al. 2015). Any observations of TC size assimilated into the reanalysis will likely improve reanalysis TC size both during and beyond the time in which data are assimilated owing to the temporal inertia associated with the improved representation of TC–environment interactions. The use of four-dimensional variational data assimilation in ERA-I and JRA-55 also allows TC size observations to directly impact the reanalysis before and after the observing time within these reanalyses (Dee et al. 2011; Kobayashi et al. 2015). Moreover, the use of TC wind profile retrievals in the JRA-55, which accounts for TC size when generating synthetic dropwindsondes, suggests that the JRA-55 may be particularly well represented even in the absence of observations (Hatsushika et al. 2006; Onogi et al. 2007; Kobayashi et al. 2015). These arguments together with the qualitative similarities (e.g., skewness and shape) among the various reanalysis TC size distribution subsets (Figs. 15 and 16) may suggest that reanalysis TC size is represented with reasonable fidelity throughout the satellite era.

4. Summary and discussion

The present study has examined the fidelity of several outer TC size metrics and the outer TC winds (i.e., azimuthal-mean 10-m azimuthal wind) for NA and WNP TCs in four reanalysis datasets through comparison with QuikSCAT data (i.e., QSCAT-R). Specifically,

Unauthenticated | Downloaded 01/17/23 09:26 PM UTC

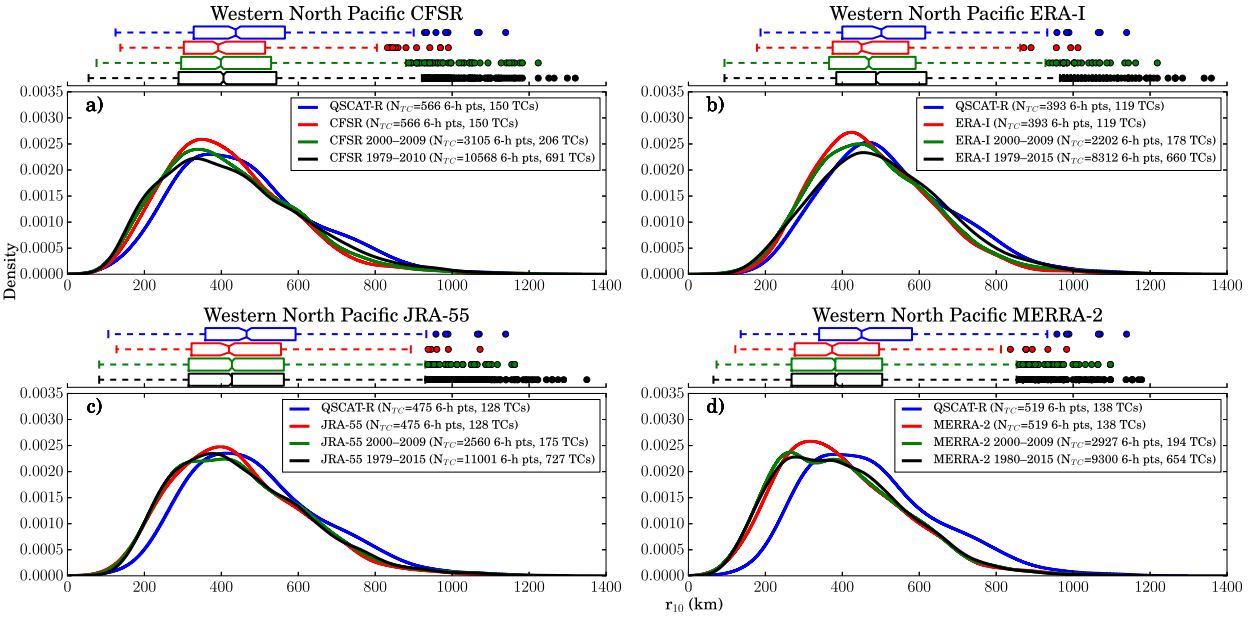

FIG. 16. As in Fig. 15, but for r_{10} (km) in WNP TCs.

r_2, r_4, r_6, r_8, r_{10}, and r_{12} in the CFSR, ERA-I, JRA-55, and MERRA-2 are compared against the QSCAT-R dataset to quantify the frequency in which reanalysis TC size is defined and how accurate and precise these estimates are. The accuracy and precision of the radial profile of azimuthal-mean 10-m azimuthal wind for reanalysis TCs are also analyzed. Trends in the difference between reanalysis and QSCAT-R TC size with QSCAT-R TC size and TC latitude are also examined. The final portion of this study investigates reanalysis TC size for all 6-h IBTrACS data points during the QSCAT-R era and satellite era. Based upon these results, the present study suggests that reanalyses can reasonably represent both outer TC size and outer TC structure not only when QuikSCAT data are available for assimilation but likely throughout the satellite era as well. In particular, the following conclusions are made for reanalysis TC size: 1) r_6–r_8 in the NA and r_6–r_8 in the WNP are the optimal choices of TC size metrics, 2) NA outer TC size and outer structure are more accurately represented than WNP TCs, and 3) the CFSR and JRA-55 generally depict outer TC size and outer structure with the greatest fidelity.

More specifically, TC size metrics with wind speed thresholds less than $10\,m\,s^{-1}$ in the NA and $12\,m\,s^{-1}$ in the WNP are most frequently defined in reanalyses given that wind speeds above these thresholds are not well resolved in reanalysis TCs. The distribution of the difference between reanalysis and QSCAT-R TC size is narrower with smaller biases for QSCAT-R TC size metrics with increasingly larger wind speed thresholds. Reanalysis TC size metrics are strongly, and statistically significantly, correlated with QSCAT-R TC size, especially for the CFSR and JRA-55. The variability of reanalysis TC size is generally close to but slightly less than QSCAT-R TC size.

Further insight is provided by examining radial profiles of the azimuthal-mean 10-m azimuthal wind revealing that wind speeds at or below $\sim 10\,m\,s^{-1}$ are strongly, and statistically significantly, correlated in each reanalysis. While reanalysis TC wind speeds are slightly underestimated consistent with the TC size results, the shape and interquartile range of the radial profile of reanalysis TC winds are very similar to QSCAT-R. These results suggest that outer TC structure is relatively well represented in reanalyses in both basins. In contrast, azimuthal-mean 10-m azimuthal winds exceeding $\sim 10\,m\,s^{-1}$ appear to show a relatively strong, nonlinear underestimation in reanalyses suggesting that r_{12} should not be studied in reanalyses. Additional analysis reveals that reanalysis TC size representation may be impacted by increases in TC size error with increasing QSCAT-R TC size in both basins and with decreasing TC latitude in the WNP.

Last, distributions of r_8 in the NA and r_{10} in the WNP from QSCAT-R are compared with the corresponding reanalysis distributions demonstrating that while both sets of distributions are approximately lognormal, the reanalysis distributions are slightly narrower and biased toward smaller values. Distributions of r_8 and r_{10} are examined in the interest of brevity given that these results are qualitatively similar to other TC size metrics

Unauthenticated | Downloaded 01/17/23 09:26 PM UTC

examined in the present study. Analysis of the reanalysis r_8 and r_{10} distribution for all 6-h IBTrACS data points during the QSCAT-R era and satellite era reveals qualitatively similar distributions with a lognormal shape, positive skewness, and similar width compared to QSCAT-R TCs, although statistical testing generally suggests statistically significant differences with QSCAT-R exist between all reanalyses except the ERA-I. The similarities between the distributions of r_8 and r_{10} for QSCAT-R TCs and for all 6-h IBTrACS TCs during the satellite era suggests that reanalysis r_8 and r_{10} may be reasonably represented during the satellite era. Together, these results suggest that reanalyses represent a long-term, objective, and homogeneous source of TC size estimates and outer TC structure that may be particularly useful for climatological studies of TC size.

Acknowledgments. This study is supported by Grants EAR-1520683 from the National Science Foundation and NA14OAR4320106 and NA15NWS4680005 from the National Oceanic and Atmospheric Administration, U.S. Department of Commerce. The statements, findings, conclusions, and recommendations herein are those of the authors and do not necessarily reflect the views of the National Science Foundation, the National Oceanic and Atmospheric Administration, or the U.S. Department of Commerce. This research has benefitted from critical and constructive input from Kelvin T. F. Chan (City U-Hong Kong), an anonymous reviewer, Robert Hart (FSU), Michael Fiorino (NOAA/ESRL), Paul Berrisford (ECMWF), and Michael Bosilovich (NASA). This work would not have been possible without the availability of the CFSR, ERA-I, JRA-55, and MERRA-2 from NCEP, ECMWF, NASA, and the JMA, respectively. We would also like to thank NCAR for providing the QSCAT-R data and postprocessed ERA-I and JRA-55 data. All computations were done in Python and figures were made using Matplotlib (Hunter 2007).

REFERENCES

Bosilovich, M., J. Kennedy, D. Dee, R. Allan, and A. O'Neill, 2013: On the reprocessing and reanalysis of observations for climate. *Climate Science for Serving Society: Research, Modeling and Prediction Priorities*, A. Ghassem and J. W. Hurrell, Eds., Springer, 51–71.

Brammer, A., 2017: Tropical cyclone vortex tracker. Zenodo, https://doi.org/10.5281/zenodo.266194.

Brand, S., 1972: Very large and very small typhoons of the western North Pacific Ocean. *J. Meteor. Soc. Japan*, **50**, 332–341, doi:10.2151/jmsj1965.50.4_332.

——, and C. P. Guard, 1979: An observational study of extratropical storms evolved from tropical cyclones in the western North Pacific. *J. Meteor. Soc. Japan*, **57**, 479–483, doi:10.2151/jmsj1965.57.5_479.

Carrasco, C. A., C. W. Landsea, and Y.-L. Lin, 2014: The influence of tropical cyclone size on its intensification. *Wea. Forecasting*, **29**, 582–590, doi:10.1175/WAF-D-13-00092.1.

Chan, K. T., and J. C. Chan, 2012: Size and strength of tropical cyclones as inferred from QuikSCAT data. *Mon. Wea. Rev.*, **140**, 811–824, doi:10.1175/MWR-D-10-05062.1.

——, and ——, 2013: Angular momentum transports and synoptic flow patterns associated with tropical cyclone size change. *Mon. Wea. Rev.*, **141**, 3985–4007, doi:10.1175/MWR-D-12-00204.1.

——, and ——, 2014: Impacts of initial vortex size and planetary vorticity on tropical cyclone size. *Quart. J. Roy. Meteor. Soc.*, **140**, 2235–2248, doi:10.1002/qj.2292.

——, and ——, 2015a: Global climatology of tropical cyclone size as inferred from QuikSCAT data. *Int. J. Climatol.*, **35**, 4843–4848, doi:10.1002/joc.4307.

——, and ——, 2015b: Impacts of vortex intensity and outer winds on tropical cyclone size. *Quart. J. Roy. Meteor. Soc.*, **141**, 525–537, doi:10.1002/qj.2374.

Chavas, D., and K. Emanuel, 2010: A QuikSCAT climatology of tropical cyclone size. *Geophys. Res. Lett.*, **37**, L18816, doi:10.1029/2010GL044558.

——, and ——, 2014: Equilibrium tropical cyclone size in an idealized state of axisymmetric radiative–convective equilibrium. *J. Atmos. Sci.*, **71**, 1663–1680, doi:10.1175/JAS-D-13-0155.1.

——, and J. Vigh, 2014: QSCAT-R: The QuikSCAT tropical cyclone radial structure dataset. NCAR Tech. Note NCAR/TN-5131STR, 25 pp., doi:10.5065/D6J67DZ4.

——, and N. Lin, 2016: A model for the complete radial structure of the tropical cyclone wind field. Part II: Wind field variability. *J. Atmos. Sci.*, **73**, 3093–3113, doi:10.1175/JAS-D-15-0185.1.

——, ——, and K. Emanuel, 2015: A model for the complete radial structure of the tropical cyclone wind field. Part I: Comparison with observed structure. *J. Atmos. Sci.*, **72**, 3647–3662, doi:10.1175/JAS-D-15-0014.1.

——, ——, W. Dong, and Y. Lin, 2016: Observed tropical cyclone size revisited. *J. Climate*, **29**, 2923–2939, doi:10.1175/JCLI-D-15-0731.1.

Dee, D., and Coauthors, 2011: The ERA-Interim reanalysis: Configuration and performance of the data assimilation system. *Quart. J. Roy. Meteor. Soc.*, **137**, 553–597, doi:10.1002/qj.828.

Demuth, J., M. DeMaria, and J. Knaff, 2006: Improvement of Advanced Microwave Sounding Unit tropical cyclone intensity and size estimation algorithms. *J. Appl. Meteor. Climatol.*, **45**, 1573–1581, doi:10.1175/JAM2429.1.

Emanuel, K., 2004: Tropical cyclone energetics and structure. *Atmospheric Turbulence and Mesoscale Meteorology*, E. Federovich, R. Rotunno, and B. Stevens, Eds., Cambridge University Press, 51–71.

——, 2005: Increasing destructiveness of tropical cyclones over the past 30 years. *Nature*, **436**, 686–688, doi:10.1038/nature03906.

Evans, C., and R. Hart, 2008: Analysis of the wind field evolution associated with the extratropical transition of Bonnie (1998). *Mon. Wea. Rev.*, **136**, 2047–2065, doi:10.1175/2007MWR2051.1.

Evans, J., and R. Hart, 2003: Objective indicators of the life cycle evolution of extratropical transition for Atlantic tropical cyclones. *Mon. Wea. Rev.*, **131**, 909–925, doi:10.1175/1520-0493(2003)131<0909:OIOTLC>2.0.CO;2.

Frank, W., and W. Gray, 1980: Radius and frequency of 15 m s^{-1} (30 kt) winds around tropical cyclones. *J. Appl. Meteor. Climatol.*, **19**, 219–223, doi:10.1175/1520-0450(1980)019<0219:RAFOMS>2.0.CO;2.

Unauthenticated | Downloaded 01/17/23 09:26 PM UTC

Gelaro, R., and Coauthors, 2017: The Modern-Era Retrospective Analysis for Research and Applications, version 2 (MERRA-2). *J. Climate*, **30**, 5419–5454, https://doi.org/10.1175/JCLI-D-16-0758.1.

Hart, R. E., J. L. Evans, and C. Evans, 2006: Synoptic composites of the extratropical transition life cycle of North Atlantic tropical cyclones: Factors determining posttransition evolution. *Mon. Wea. Rev.*, **134**, 553–578, doi:10.1175/MWR3082.1.

Hatsushika, H., J. Tsutsui, M. Fiorino, and K. Onogi, 2006: Impact of wind profile retrievals on the analysis of tropical cyclones in the JRA-25 reanalysis. *J. Meteor. Soc. Japan*, **84**, 891–905, doi:10.2151/jmsj.84.891.

Hodges, K., A. Cobb, and P. L. Vidale, 2017: How well are tropical cyclones represented in reanalysis datasets? *J. Climate*, **30**, 5243–5264, https://doi.org/10.1175/JCLI-D-16-0557.1.

Hunter, J. D., 2007: Matplotlib: A 2D graphics environment. *Comput. Sci. Eng.*, **9**, 90–95, doi:10.1109/MCSE.2007.55.

Iman, R. L., M. E. Johnson, and C. C. Watson, 2005: Sensitivity analysis for computer model projections of hurricane losses. *Risk Anal.*, **25**, 1277–1297, doi:10.1111/j.1539-6924.2005.00673.x.

Irish, J. L., and D. T. Resio, 2010: A hydrodynamics-based surge scale for hurricanes. *Ocean Eng.*, **37**, 69–81, doi:10.1016/j.oceaneng.2009.07.012.

——, ——, and J. J. Ratcliff, 2008: The influence of storm size on hurricane surge. *J. Phys. Oceanogr.*, **38**, 2003–2013, doi:10.1175/2008JPO3727.1.

Kimball, S., and M. Mulekar, 2004: A 15-year climatology of North Atlantic tropical cyclones. Part I: Size parameters. *J. Climate*, **17**, 3555–3575, doi:10.1175/1520-0442(2004)017<3555:AYCONA>2.0.CO;2.

Kitabatake, N., 2011: Climatology of extratropical transition of tropical cyclones in the western North Pacific defined by using cyclone phase space. *J. Meteor. Soc. Japan*, **89**, 309–325, doi:10.2151/jmsj.2011-402.

Knaff, J., and R. Zehr, 2007: Reexamination of tropical cyclone wind–pressure relationships. *Wea. Forecasting*, **22**, 71–88, doi:10.1175/WAF965.1.

——, S. P. Longmore, and D. A. Molenar, 2014: An objective satellite-based tropical cyclone size climatology. *J. Climate*, **27**, 455–476, doi:10.1175/JCLI-D-13-00096.1.

Knapp, K. R., M. C. Kruk, D. H. Levinson, H. J. Diamond, and C. J. Neumann, 2010: The international best track archive for climate stewardship (IBTrACS) unifying tropical cyclone data. *Bull. Amer. Meteor. Soc.*, **91**, 363–376, doi:10.1175/2009BAMS2755.1.

Kobayashi, S., and Coauthors, 2015: The JRA-55 reanalysis: General specifications and basic characteristics. *J. Meteor. Soc. Japan*, **93**, 5–48, doi:10.2151/jmsj.2015-001.

Kossin, J., K. Knapp, D. Vimont, R. Murnane, and B. Harper, 2007a: A globally consistent reanalysis of hurricane variability and trends. *Geophys. Res. Lett.*, **34**, L04815, https://doi.org/10.1029/2006GL028836.

——, and Coauthors, 2007b: Estimating hurricane wind structure in the absence of aircraft reconnaissance. *Wea. Forecasting*, **22**, 89–101, doi:10.1175/WAF985.1.

Landsea, C., and J. L. Franklin, 2013: Atlantic hurricane database uncertainty and presentation of a new database format. *Mon. Wea. Rev.*, **141**, 3576–3592, doi:10.1175/MWR-D-12-00254.1.

——, B. Harper, K. Hoarau, and J. Knaff, 2006: Can we detect trends in extreme tropical cyclones? *Science*, **313**, 452–453, doi:10.1126/science.1128448.

Lee, C.-S., K. K. Cheung, W.-T. Fang, and R. L. Elsberry, 2010: Initial maintenance of tropical cyclone size in the western North Pacific. *Mon. Wea. Rev.*, **138**, 3207–3223, doi:10.1175/2010MWR3023.1.

Lin, N., and D. Chavas, 2012: On hurricane parametric wind and applications in storm surge modeling. *J. Geophys. Res.*, **117**, D09120, https://doi.org/10.1029/2011JD017126.

——, and K. Emanuel, 2016: Grey swan tropical cyclones. *Nature*, **6**, 106–111, https://doi.org/10.1038/nclimate2777.

——, P. Lane, K. A. Emanuel, R. M. Sullivan, and J. P. Donnelly, 2014: Heightened hurricane surge risk in northwest Florida revealed from climatological-hydrodynamic modeling and paleorecord reconstruction. *J. Geophys. Res. Atmos.*, **119**, 8606–8623, https://doi.org/ 10.1002/2014JD021584.

Liu, K., and J. C. Chan, 1999: Size of tropical cyclones as inferred from *ERS-1* and *ERS-2* data. *Mon. Wea. Rev.*, **127**, 2992–3001, doi:10.1175/1520-0493(1999)127<2992:SOTCAI>2.0.CO;2.

Liu, Q., T. Marchok, H. Pan, M. Bender, and S. Lord, 2000: Improvements in hurricane initialization and forecasting at NCEP with global and regional (GFDL) models. NOAA Technical Procedures Bulletin 472, 7 pp.

Manning, D., and R. Hart, 2007: Evolution of North Atlantic ERA40 tropical cyclone representation. *Geophys. Res. Lett.*, **34**, L05705, https://doi.org/10.1029/2006GL028266.

Marchok, T. P., 2002: How the NCEP tropical cyclone tracker works. *25th Conf. on Hurricanes and Tropical Meteorology*, San Diego, CA, Amer. Meteor. Soc., P1.13, https://ams.confex.com/ams/25HURR/techprogram/paper_37628.htm.

Merrill, R., 1984: A comparison of large and small tropical cyclones. *Mon. Wea. Rev.*, **112**, 1408–1418, doi:10.1175/1520-0493(1984)112<1408:ACOLAS>2.0.CO;2.

Murakami, H., 2014: Tropical cyclones in reanalysis data sets. *Geophys. Res. Lett.*, **41**, 2133–2141, doi:10.1002/2014GL059519.

Nguyen, L. T., J. Molinari, and D. Thomas, 2014: Evaluation of tropical cyclone center identification methods in numerical models. *Mon. Wea. Rev.*, **142**, 4326–4339, doi:10.1175/MWR-D-14-00044.1.

Onogi, K., and Coauthors, 2007: The JRA-25 reanalysis. *J. Meteor. Soc. Japan*, **85**, 369–432, doi:10.2151/jmsj.85.369.

Parker, W. S., 2016: Reanalyses and observations: What's the difference? *Bull. Amer. Meteor. Soc.*, **97**, 1565–1572, doi:10.1175/BAMS-D-14-00226.1.

Reed, K., and C. Jablonowski, 2011: Impact of physical parameterizations on idealized tropical cyclones in the Community Atmosphere Model. *Geophys. Res. Lett.*, **38**, L04805, https://doi.org/10.1029/2010GL046297.

——, and ——, 2012: Idealized tropical cyclone simulations of intermediate complexity: A test case for AGCMs. *J. Adv. Model. Earth Syst.*, **4**, M04001, https://doi.org/10.1029/2011MS000099.

——, ——, and M. A. Taylor, 2012: Tropical cyclones in the spectral element configuration of the Community Atmosphere Model. *Atmos. Sci. Lett.*, **13**, 303–310, doi:10.1002/asl.399.

Ryglicki, D. R., and R. E. Hart, 2015: An investigation of center-finding techniques for tropical cyclones in mesoscale models. *J. Appl. Meteor. Climatol.*, **54**, 825–846, doi:10.1175/JAMC-D-14-0106.1.

——, and D. Hodyss, 2016: A deeper analysis of center-finding techniques for tropical cyclones in mesoscale models. Part I: Low-wavenumber analysis. *J. Appl. Meteor. Climatol.*, **55**, 531–559, doi:10.1175/JAMC-D-15-0125.1.

Saha, S., and Coauthors, 2010: The NCEP Climate Forecast System Reanalysis. *Bull. Amer. Meteor. Soc.*, **91**, 1015–1057, doi:10.1175/2010BAMS3001.1.

Schenkel, B., and R. Hart, 2012: An examination of tropical cyclone position, intensity, and intensity life cycle within

Unauthenticated | Downloaded 01/17/23 09:26 PM UTC

atmospheric reanalysis datasets. *J. Climate*, **25**, 3453–3475, doi:10.1175/2011JCLI4208.1.

——, and ——, 2015a: An analysis of the environmental moisture impacts of western North Pacific tropical cyclones. *J. Climate*, **28**, 2600–2622, doi:10.1175/JCLI-D-14-00213.1.

——, and ——, 2015b: An examination of the thermodynamic impacts of western North Pacific tropical cyclones on their tropical tropospheric environment. *J. Climate*, **28**, 7529–7560, doi:10.1175/JCLI-D-14-00780.1.

Skamarock, W. C., 2004: Evaluating mesoscale NWP models using kinetic energy spectra. *Mon. Wea. Rev.*, **132**, 3019–3032, doi:10.1175/MWR2830.1.

Sriver, R., and M. Huber, 2006: Low frequency variability in globally integrated tropical cyclone power dissipation. *Geophys. Res. Lett.*, **33**, 1986–2005, doi:10.1029/2006GL026167.

Stiles, B., and Coauthors, 2014: Optimized tropical cyclone winds from QuikSCAT: A neural network approach. *IEEE Trans. Geosci. Remote Sens.*, **52**, 7418–7434, doi:10.1109/TGRS.2014.2312333.

Thorne, P., and R. Vose, 2010: Reanalyses suitable for characterizing long-term trends: Are they really achievable? *Bull. Amer. Meteor. Soc.*, **91**, 353–361, doi:10.1175/2009BAMS2858.1.

Truchelut, R., and R. Hart, 2011: Quantifying the possible existence of undocumented Atlantic warm-core cyclones in NOAA/CIRES 20th Century Reanalysis data. *Geophys. Res. Lett.*, **38**, L08811, https://doi.org/10.1029/2011GL046756.

——, ——, and B. Luthman, 2013: Global identification of previously undetected pre-satellite-era tropical cyclone candidates in NOAA/CIRES Twentieth-Century Reanalysis data. *J. Appl. Meteor. Climatol.*, **52**, 2243–2259, doi:10.1175/JAMC-D-12-0276.1.

Vecchi, G., and T. Knutson, 2008: On estimates of historical North Atlantic tropical cyclone activity. *J. Climate*, **21**, 3580–3600, doi:10.1175/2008JCLI2178.1.

Weatherford, C., and W. Gray, 1988a: Typhoon structure as revealed by aircraft reconnaissance. Part I: Data analysis and climatology. *Mon. Wea. Rev.*, **116**, 1032–1043, doi:10.1175/1520-0493(1988)116<1032:TSARBA>2.0.CO;2.

——, and ——, 1988b: Typhoon structure as revealed by aircraft reconnaissance. Part II: Structural variability. *Mon. Wea. Rev.*, **116**, 1044–1056, doi:10.1175/1520-0493(1988)116<1044:TSARBA>2.0.CO;2.

Wood, K. M., and E. A. Ritchie, 2014: A 40-year climatology of extratropical transition in the eastern North Pacific. *J. Climate*, **27**, 5999–6015, doi:10.1175/JCLI-D-13-00645.1.

Zhai, A. R., and J. H. Jiang, 2014: Dependence of US hurricane economic loss on maximum wind speed and storm size. *Environ. Res. Lett.*, **9**, 064019, https://doi.org/10.1088/1748-9326/9/6/064019.

Unauthenticated | Downloaded 01/17/23 09:26 PM UTC